J Nanostruct 10(4): 802-809, Autumn 2020

RESEARCH PAPER

Comparative Photocatalytic Performance of TiO_2 and TiO_2/en-MIL-101 (Cr) for Degradation of Rhodamine B as a Model of Pollutant under UV and Visible Irradiations

***Mahdi Abroudi*[1], *Amir Homayoun Keihan*[2]**

[1]*Student Research Committee, Baqiyatallah University of Medical Sciences, Tehran, Iran*

[2]*Molecular Biology Research Center, Systems Biology and Poisonings Institute, Baqiyatallah University of Medical Sciences, Tehran, Iran*

ARTICLE INFO

Article History:
Received 24 July 2020
Accepted 11 September 2020
Published 01 December 2020

Keywords:
Dye degradation
Metal–organic frameworks
Photocatalyst
TiO_2/en-MIL-101(Cr)

ABSTRACT

In this research, a new photocatalyst of TiO_2 /en-MIL-101 (Cr) was synthesized via hydrothermal method. The as-prepared hetrostructure material was characterized by X-ray diffraction, Fourier Transform Infrared Spectrometer, energy dispersive X-ray spectroscopy, ultraviolet-visible diffuse reflection spectra, scanning and transmission electron microscopy. The photodegradation of rhodamine B by the synthesized photocatalysts was investigated under UV irradiation and visible light. The results showed that immobilization of TiO_2 on the surface and inside the photocatalytic structure enhanced the degradation of the pollutant. The band gap energy of the synthesized TiO_2 /en-MIL-101(Cr) measured by ultraviolet-visible diffuse reflection spectra showed that an insignificant shift to lower energy was situated after immobilization onto the structure of the supports. The relationship between the photocatalytic activity and the structure of TiO_2 /en-MIL-101(Cr) hetrostructure was discussed. The degradation efficiency of 84% and 77% of rhodamine B was respectively obtained by TiO_2/en-MIL-101(Cr) under Uv and visible light, respectively. This work has introduced a new way for using the MOF in the design of photocatalyst substrate for organic dyes degradation in waste water.

How to cite this article
Abroudi M., AKeihan A.H. Comparative Photocatalytic Performance of TiO_2 and TiO_2 /en-MIL-101 (Cr) for Degradation of Rhodamine B as a Model of Pollutant under UV and Visible Irradiations. J Nanostruct, 2020; 10(4): 802-809. DOI: 10.22052/JNS.2020.04.013

INTRODUCTION

The semiconductor photocatalytic degradation of various environmental pollutants such as dyes is very important for the development of the sustainable environment and energy[1, 2]. Various semiconductors such as WO_3[3], TiO_2, ZnO, ZnWO4 and CdS have been widely used for photocatalysis[4-7]. Semiconductor photocatalysts can convert sun light from the sun to chemical energy. When electrons in the valence band given an energy equal or greater than the band gap it will be excited to the conduction band and generated charge carrier[8, 9]. The electron –hole pairs can generate free radicals like hydroxyl (. OH) or superoxide anion radicals as an active space for the degradation process[10, 11]. Among various semiconductor photocatalysts, titanium dioxide (TiO_2) is the most commonly used for photocatalyst because of its nontoxicity, inexpensive, green and highly chemical stability[12]. However, TiO_2 have a wide band gap (3.2 eV for anatase and 3.0 eV for rutile) which only a very small fraction (5%) of the solar energy falls in the UV region. Furthermore, TiO_2 has a low quantum yield, rapid charge carrier recombination (electron-hole) and high energy consumption[13-15]. Therefore, it is essential

* *Corresponding Author Email: ahkeihan@bmsu.ac.ir*

to development of new suitable structures for enhanced photocatalytic performances and efficient use of visible light. Supporting of semiconductors onto a suitable support such as zeolites and metal–organic frameworks (MOFs) will be the most and effectual procedure to dominate recombination of photogenerated electron–hole[16-18].

Metal–organic frameworks (MOFs) are crystalline and new kind of inorganic/organic hybrid have attracted research attention. The fascinating diverse structures, high surface area, permanent nanoscale porosity, topologies and uniform structured cavities make MOFs appropriate for a wide range of applications such as sensors, drug delivery, gas separation, gas storage and photocatalysis[19-23]. Metal–organic frameworks (MOFs) has uniform pore structure and become semiconductors when exposed to light, thus making MOFs potentially by heterogeneous photocatalysts for degradation environmental pollutants due to their uniform pore structure, high crystallinity, high specific surface area, organic linkers and tailorable structure[24-26].

Herein, we report new photocatalysts by immobilization of TiO_2 on the surface and encapsulated of embedded MIL-101 ($Cr_3F(H_2O)_2O[BDC]_3$. nH_2O, BDC = terephthalic acid) for degradation of rhodamine B as an organic pollutant under Uv and visible light. The resulting TiO_2/ en-MIL-101 was characterized by FT-IR, XRD, FE-SEM, EDS, TEM and UV-vis DRS spectroscopy. The photocatalytic activities of the TiO_2/en-MIL-101 composites were evaluated by degradation of rhodamine B under UV and visible-light.

MATERIALS AND METHODS

Tetra butyltitanate, N, N-dimethyl-formamide (99%) (DMF), Chromic nitrate, TiO_2 (P25), nonahydrate ($Cr(NO_3)_3{\cdot}9H_2O$, ethylenediamine, Toluene, methanol, isopropanol (99.7%) from Sigma Aldrich. Terephthalic acid (H_2BDC, ≥99.0%) from Shanghai KEFENG Chemical Reagent Co., Ltd. Deionized water was prepared by an ultra-pure water system (Smart-2-Pure, TKA Co, Germany). Rhodamine B (Rh B) was provided by Alvan Co, Iran. All chemical materials used in this study were of commercially available analytical grade and used without further purification.

Phase's analyses of the prepared samples were carried out by powder XRD (Philips X'pert Pro MPD, Holland) using graphite-filtered Cu K α (k=0.154 nm) radiation in the range of 2θ from 10 to 80 with a 2θ step size of 0.021 and a measuring time of 0.8 s per point. SEM images were obtained using an LEO instrument model 1455VP with an energy dispersive X-ray detector (EDX, EDAX Genenis- 4000, USA) operated at 25 kV with spot size 4. FT Infrared (FT-IR) spectra were obtained as potassium bromide pellets in the range of 400–4000 cm-1 with a Nicolet- Impact 400 D spectrophotometer. Band gap was obtained by UV spectra of the samples were recorded by UV–Vis DRS spectrophotometer (Shimadzu, model UV-3101) with the scan rate 5 nm s^{-1}. The UV-Vis spectra of the samples were taken on a UV-Vis spectrophotometer (Shimadzu, UV-2550, Japan) visible sources of 400 W Osram lamps.

Preparation of en-MIL-101 (Cr)

en-MIL-101 (Cr) prepared by hydrothermal method. Briefly 2 g of chromium nitrate and 0.85 g Terephthalic acid were slowly added to 24 mL of deionized water. The resulting mixture was stirred for 30 min and transferred into a Teflon-lined stainless steel autoclave. The autoclave was heated at 180 ◦C for 18 h. After cooling autoclave, the suspension was centrifuged and the solid was separated, washed respectively with 20 mL of DMF, H_2O and Me(OH), and dried at 80 ◦C. The product was designated as MIL-101(Cr).

To modify MIL-101(Cr) with ethylenediamine, 0.10 g MIL-101(Cr) was first dispersed in 20 mL dry toluene in a flask and 0.04 mL ethylenediamine added to the mixture, then solution was refluxed at 110 ◦C for 18 h. After this step, the precipitated was washed with water and methanol three times and dried at 80 ◦C for 24 h.

Preparation of TiO_2/ en-MIL-101 (Cr)

For immobilize TiO_2 on the surface, 0.50 g of as-synthesized en-MIL-101 (Cr) was dispersed in 20 mL of methanol by ultrasonic and then 1 mL of tetra butyltitanate was added to the mixture. The mixture was refluxed at 65 ◦C for 10 h. Finally, the suspension was centrifuged and the solid was removed, washed three times with deionized water and methanol, then dried at 60 ◦C for 12 h.

Photocatalytic Performance

Photocatalytic activity of samples was evaluated by degradation of rhodamine B (RhB) as a model of water pollutant under UV and visible light irradiation.

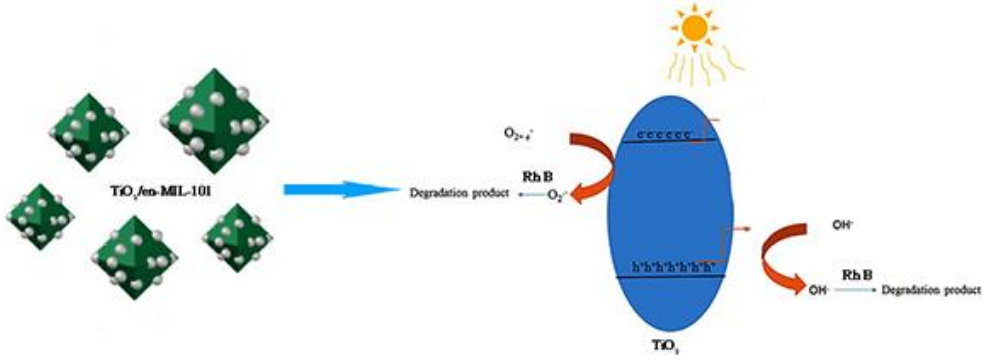

Fig.1. Schematic of catalysts structure and mechanism of catalyst performance.

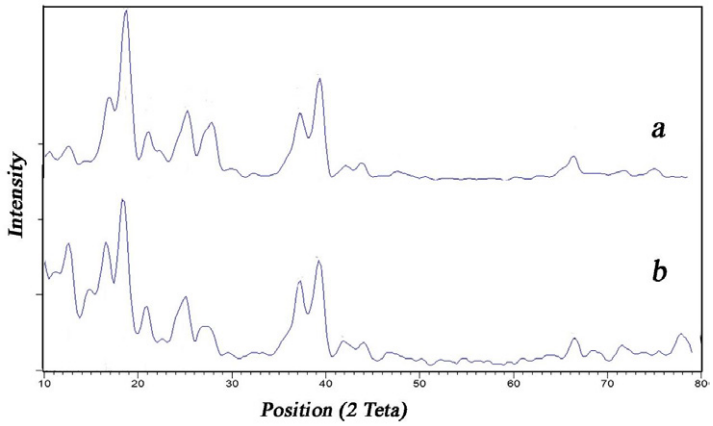

Fig2. XRD pattern of (a) en-MIL-101 (Cr) (b) TiO_2/en-MIL-101 (Cr)

The photocatalytic degradation occurred with 50 ml of RhB aqueous solution with a concentration of 10 ppm and 0.05 g of photocatalyst in a quartz tube. Two 400 W lamps were utilized as a light source for visible and UV sources. The quartz tube is located 40 cm and 30 cm away for UV and visible from source, respectively. The mixture of photocatalyst nanoparticles was aerated and stirred in the dark for 30 min to reach adsorption equilibrium. Then mixture in quartz tube is placed under the UV or visible lamp irradiation, centrifuged and analyzed with the UV–vis spectrometer. Percent of the RhB degradation in time of t (DP (t)) was calculated as follows:

$$DP(t) = \frac{A_0 - A_t}{A_0} \times 100 \quad (1)$$

In this equation, A_0 and A_t are the absorbance value of the solution at 0 and t minute, respectively. Fig. 1 shows the schematic of the formation and photocatalysts performance of TiO_2/ en-MIL-101 (Cr) nanocomposite.

RESULTS AND DISCUSSION

Characterization of the synthesized photocatalysts

The phase and structure samples were examined by X-ray powder diffraction (XRD). Fig. 2a shows the XRD analysis of the formation of en-MIL-101 (Cr). As shown in Fig. 2, en-MIL-101 (Cr) display characteristic diffraction peaks of MIL-101, which was in analogous with the offered in the literature [27]. The crystallographic structure and phase purity of the TiO_2/en-MIL-101 is not only evident loss of crystallinity, but also the TiO_2/en-MIL-101 (Cr) showed privileged diffraction peaks 2θ = 25.67, 38 .8 and 44.20 corresponding to the anatase phase of TiO_2 (JCPDS card No: 04-0477). Furthermore, the XRD data of TiO_2/en-MIL-101 (Cr) clearly shows the composite has been successfully synthesized by hydrothermal method.

The FT-IR spectra of en-MIL-101 (Cr) and TiO_2/en-MIL-101 (Cr) are given in Fig. 3. For en-MIL-101 (Cr), the peak at 3620 cm^{-1} is clearly observed, which is related to the asymmetrical stretching vibration of the amine groups. In the

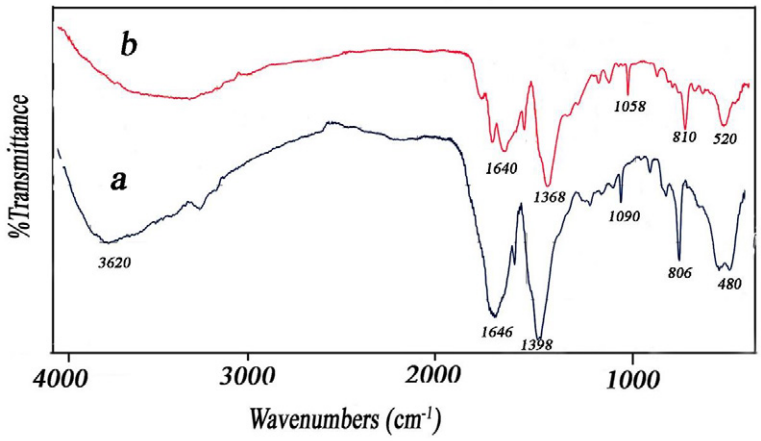

Fig3. FTIR spectra of (a) en-MIL-101 (Cr) (b) TiO_2/en-MIL-101 (Cr)

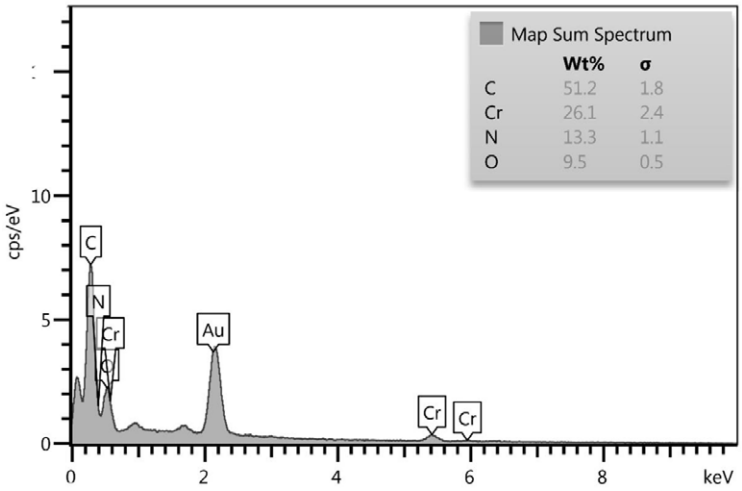

Fig.4. EDS data of en-MIL-101 (Cr)

lower frequency region, the peak around 1640 cm^{-1} related to the N–H bending vibration. The absorption bands revealed at 1640, 1646, 3607 and 3620 cm^{-1} are related to the bending and stretching vibration modes of the hetrostructure water. The peaks at 1058cm^{-1} and 520 cm^{-1} shows that a Ti–O stretching into the structure of en-MIL-101 (Cr) hetrostructure. The broad strong band below 1100cm^{-1} is due to Ti-O-Ti vibration. In the region below 1000cm^{-1}, band of Cr-O appears about 480 cm^{-1}.

The EDS data of en-MIL-101 (Cr) hetrostructure sample is shown in Fig. 4. The EDS spectrum shows that the sample is composed of O, N, Cr and C in the catalyst structure. Since in coating by Au for preparation of EDS and SEM images, some peaks appear in the spectrum.

The morphology of en-MIL-101 (Cr)and TiO2/en-MIL-101 (Cr) hetrostructure was investigated by scanning electron microscopy and the corresponding SEM images are demonstrate in Fig. 5. The grains are found to be uniform particle, homogenously dispersed and slightly agglomerated. In the SEM image of en-MIL-101 (Cr), well defined cubic grain like crystals and particles size about 60-100 nm were observed. In the image of TiO_2/en-MIL-101(Cr) the cubic crystals were observed denoting that the en-MIL-101(Cr) did not affected by TiO_2 loading. The SEM image indicates that the morphology of the

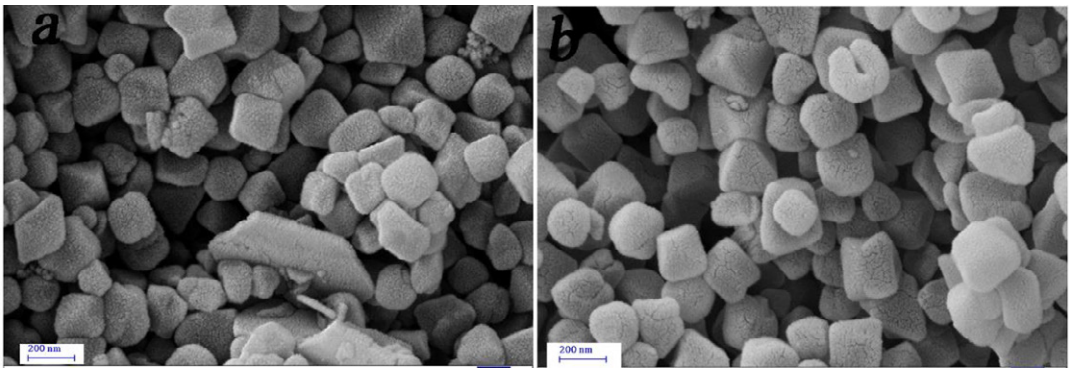

Fig.5. SEM images of (a) en-MIL-101 (Cr) (b) TiO_2/en-MIL-101 (Cr)

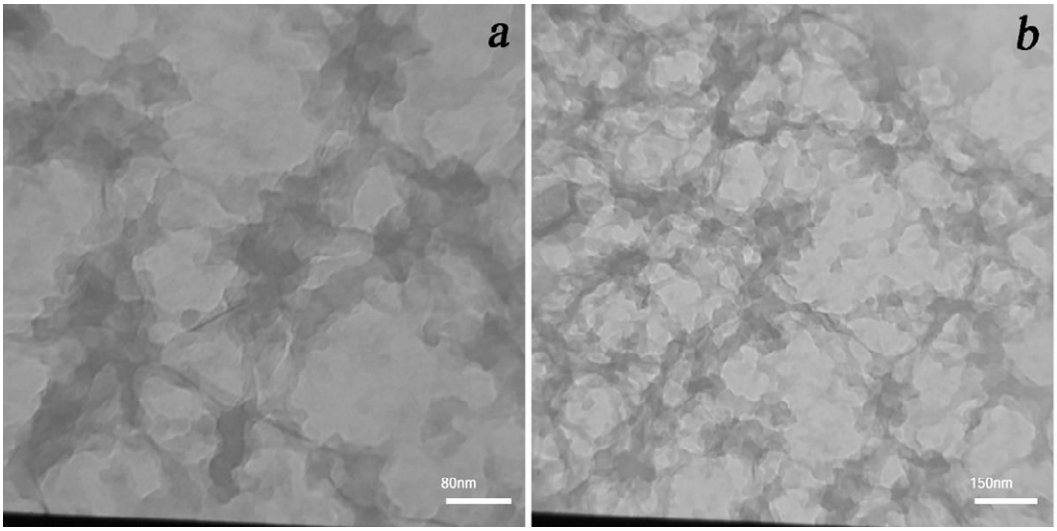

Fig.6. TEM images of (a) en-MIL-101 (Cr) (b) TiO_2/en-MIL-101 (Cr)

samples is very rough, increases surface area and enhancing photocatalyst activity. Fig. 5b shows the SEM images of TiO_2/en-MIL-101(Cr), denoting the well integrating between the TiO_2 nanoparticles and the MIL-101.

For a more detailed of the surface photocatalyst, morphologies and particle sizes of sample TiO_2/en-MIL-101(Cr), were considered by transmission electron microscopy (TEM). As showed in Fig. 6 TEM images showed that en-MIL-101(Cr) and TiO_2/en-MIL-101(Cr) samples have about cubic shape, not agglomeration and narrow size distribution with an average size of 50-90 nm. It is seen that TiO_2 aggregates can be formed on the external surface and into the cubic structure of MIL-101 crystals.

Optical property and photocatalytic activity is depended to band gap of photocatalyst. The Kubelka–Munk function versus band gap energy is shown in Fig. 7. The reflectance (R%) obtained from DRS spectra of TiO_2/en-MIL-101(Cr) were used for calculation of band gap energy of the photocatalysts by use of Kubelka-Munk and Tauc plots. As shown in theFig. 7b, a slightly decrease in the band gap energy of TiO_2/en-MIL-101(Cr) compared to bulk TiO_2 was observed. The shift was from 3.25 to 3.10 eV denoting that the immobilization of TiO_2 into structure and on surface of the en-MIL-101(Cr) structure lowered the bang gap energy of the photocatalyst. The shift to the lower energy is very important for degradation of pollutant under sun (visible) light irradiation [20]. Also, intensity of the DRS Peak of TiO_2/en-MIL-101(Cr) showed that the electron-hole recombination was reduce. This is very useful for degradation of the pollutant under Uv and

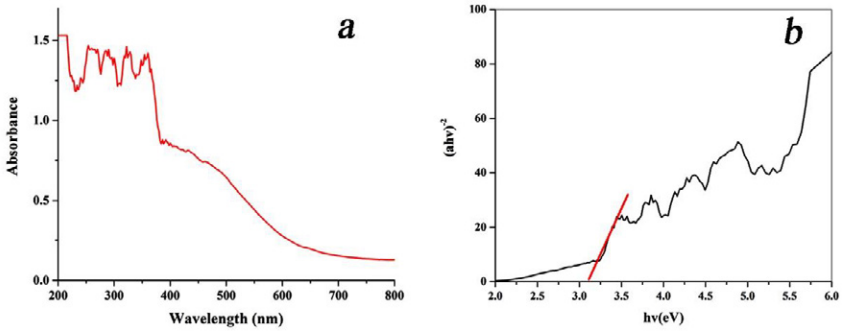

Fig.7. UV–Vis DRS spectra of TiO_2/en-MIL-101 (Cr) photocatalysts.

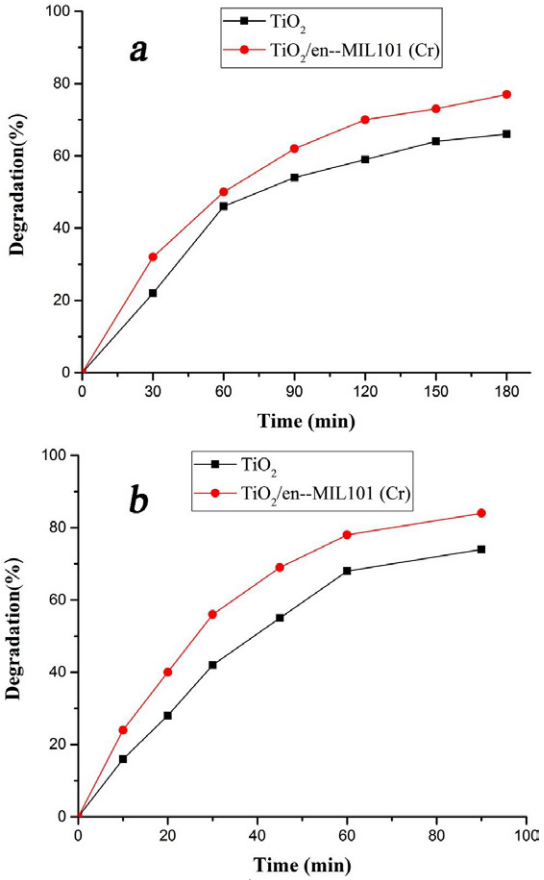

Fig.8. Plot of percentage degradation of RhB by P25 and TiO_2/en-MIL-101 (Cr) photocatalysts under (a) visible (b) UV irradiation.

visible light.

Without photocatalyst, degradation of rhodamine B under UV and visible irradiation was less than 4% comparing with primary concentration. Also for investigation of adsorption–desorption equilibrium of dye on the surface of catalysts, photocatalyst and Rhodamine B mixed and stirred in dark condition for 30 minutes, there was no dye degradation. To investigate the photocatalytic activity of heterostructure, we compared the degradation of Rhodamine B using TiO_2/en-MIL-101(Cr) and TiO_2 (P25). The visible and Uv light photoactivity of TiO_2/en-MIL-101(Cr) and TiO_2 shown in Figs 8a and b, respectively. According to observed, the time for complete was 180 min under visible irradiation, while the TiO_2/

en-MIL-101(Cr) and P25 decompose 77% and 66% of dye during the same time. Degradation of Rhodamine B after 90 min under UV irradiation was investigation in Fig. 8a and b. It is obvious that under the UV irradiation TiO_2/en-MIL-101(Cr) and P25 are the best catalysts and degradation is 84% and 74%, respectively. TiO_2/en-MIL-101(Cr) photocatalyst showed higher activity than P25. This was coincident with the result obtained by band gap energy in DRS study. The lower band gap in TiO_2/en-MIL-101(Cr) implied that the photocatalyst activity increases by visible light. Also, the TiO_2 particle on the support increased the surface area of the photocatalysis which increased higher and more adsorption of the rhodamine B over the photocatalysis surface. Also, intensity of the DRS Peak of TiO_2/en-MIL-101(Cr) indicating that the electron/hole recombination was lowered. This may be attributed to homogenous distribution of the generated electrons/hole throughout the photocatalyst structure.

CONCLUSIONS

In this study, first en-MIL-10 (Cr) were synthesized by hydrothermal method and then placing of TiO_2 into structure of en-MIL-101(Cr) photocatalysts were prepared and were used for degradation of Rhodamine B by visible and Uv light. Hetrostructure photocatalysts were confirmed by XRD, FE-SEM, TEM, Uv–vis DRS and FT-IR analyses. Stabilizing TiO2 nanoparticle into the en-MIL-10 (Cr) caused increased the surface area of the photocatalysts which increased higher and more adsorption of the rhodamine B over the photocatalyst surface. The photocatalytic activity results showed that the TiO_2/en-MIL-101(Cr) enhancement photocatalytic activity and stability in the degradation of Rh B than to TiO_2 nanoparticles. Due to its high activity, such as high surface area of the photocatalysts, low-cost and low electron/hole recombination, the TiO_2/en-MIL-101(Cr) is an excellent photocatalyst for the photodegradation of organic pollutants in wastewater under UV and visible light. This work provides a new method using TiO_2/en-MIL-101(Cr) under UV and visible light for photodegradation of organic pollutant for environmental purification.

CONFLICT OF INTEREST

The authors declare that there is no conflict of interests regarding the publication of this manuscript.

REFERENCES

1. Houas A, Lachheb H, Ksibi M, Elaloui E, Guillard C, Herrmann J-M. Photocatalytic degradation pathway of methylene blue in water. Applied Catalysis B: Environmental. 2001;31(2):145-157.
2. Chatterjee D, Dasgupta S. Visible light induced photocatalytic degradation of organic pollutants. Journal of Photochemistry and Photobiology C: Photochemistry Reviews. 2005;6(2-3):186-205.
3. Chen D, Gao L, Yasumori A, Kuroda K, Sugahara Y. Size- and Shape-Controlled Conversion of Tungstate-Based Inorganic-Organic Hybrid Belts to WO3Nanoplates with High Specific Surface Areas. Small. 2008;4(10):1813-22.
4. Mazhari MP, Abbasi A, Derakhshan A, Ahmadi M. Fabrication $Fe_3O_4/SiO_2/TiO_2$ nanocomposites and degradation of rhodamine b dyes under uv light irradiation. Journal of Nanostructures. 2016;6(1):-.
5. Mazhari M-P, Hamadanian M, Mehipour M, Jabbari V. Central composite design (CCD) optimized synthesis of Fe3O4@SiO2@AgCl/Ag/Ag2S as a novel magnetic nano-photocatalyst for catalytic degradation of organic pollutants. Journal of Environmental Chemical Engineering. 2018;6(6):7284-93.
6. Georgekutty R, Seery MK, Pillai SC. A Highly Efficient Ag-ZnO Photocatalyst: Synthesis, Properties, and Mechanism. The Journal of Physical Chemistry C. 2008;112(35):13563-70.
7. Huang G, Zhu Y. Synthesis and photocatalytic performance of ZnWO4 catalyst. Materials Science and Engineering: B. 2007;139(2-3):201-8.
8. Zhang H, Lv X, Li Y, Wang Y, Li J. P25-Graphene Composite as a High Performance Photocatalyst. ACS Nano. 2009;4(1):380-6.
9. Han L, Xu Z, Wang P, Dong S. Facile synthesis of a free-standing Ag@AgCl film for a high performance photocatalyst and photodetector. Chemical Communications. 2013;49(43):4953.
10. Yun HJ, Lee H, Joo JB, Kim ND, Yi J. Tuning the band-gap energy of TiO2-xCx nanoparticle for high performance photo-catalyst. Electrochemistry Communications. 2010;12(6):769-72.
11. Islam MJ, Reddy DA, Ma R, Kim Y, Kim TK. Reduced-graphene-oxide-wrapped BiOI-AgI heterostructured nanocomposite as a high-performance photocatalyst for dye degradation under solar light irradiation. Solid State Sciences. 2016;61:32-39.
12. Khojasteh H, Salavati-Niasari M, Mazhari M-P, Hamadanian M. Preparation and characterization of Fe3O4@SiO2@TiO2@Pd and Fe3O4@SiO2@TiO2@Pd–Ag nanocomposites and their utilization in enhanced degradation systems and rapid magnetic separation. RSC Advances. 2016;6(81):78043-52.
13. Schneider J, Matsuoka M, Takeuchi M, Zhang J, Horiuchi Y, Anpo M, et al. Understanding TiO2Photocatalysis: Mechanisms and Materials. Chemical Reviews. 2014;114(19):9919-86.
14. Nakata K, Fujishima A. TiO2 photocatalysis: Design and applications. Journal of Photochemistry and Photobiology C: Photochemistry Reviews. 2012;13(3):169-89.
15. Reutergådh LB, Iangphasuk M. Photocatalytic decolourization of reactive azo dye: A comparison between TiO2 and us photocatalysis. Chemosphere. 1997;35(3):585-96.

16. Liu X, Dang R, Dong W, Huang X, Tang J, Gao H, et al. A sandwich-like heterostructure of TiO 2 nanosheets with MIL-100(Fe): A platform for efficient visible-light-driven photocatalysis. Applied Catalysis B: Environmental. 2017;209:506-13.
17. Zhu S-R, Wu M-K, Zhao W-N, Yi F-Y, Tao K, Han L. Fabrication of heterostructured BiOBr/Bi24O31Br10/TiO2 photocatalyst by pyrolysis of MOF composite for dye degradation. Journal of Solid State Chemistry. 2017;255:17-26.
18. Li J, Xu X, Liu X, Qin W, Wang M, Pan L. Metal-organic frameworks derived cake-like anatase/rutile mixed phase TiO2 for highly efficient photocatalysis. Journal of Alloys and Compounds. 2017;690:640-6.
19. Furukawa H, Cordova KE, O'Keeffe M, Yaghi OM. The Chemistry and Applications of Metal-Organic Frameworks. Science. 2013;341(6149):1230444.
20. Czaja AU, Trukhan N, Müller U. Industrial applications of metal–organic frameworks. Chemical Society Reviews. 2009;38(5):1284-1293.
21. Mueller U, Schubert M, Teich F, Puetter H, Schierle-Arndt K, Pastré J. Metal–organic frameworks—prospective industrial applications. J Mater Chem. 2006;16(7):626-36.
22. Kuppler RJ, Timmons DJ, Fang Q-R, Li J-R, Makal TA, Young MD, et al. Potential applications of metal-organic frameworks. Coordination Chemistry Reviews. 2009;253(23-24):3042-66.
23. Liu J, Chen L, Cui H, Zhang J, Zhang L, Su C-Y. Applications of metal–organic frameworks in heterogeneous supramolecular catalysis. Chem Soc Rev. 2014;43(16):6011-61.
24. Jiang H-L, Xu Q. Porous metal–organic frameworks as platforms for functional applications. Chemical Communications. 2011;47(12):3351.
25. Morozan A, Jaouen F. Metal organic frameworks for electrochemical applications. Energy & Environmental Science. 2012;5(11):9269.
26. Bai Y, Dou Y, Xie L-H, Rutledge W, Li J-R, Zhou H-C. Zr-based metal–organic frameworks: design, synthesis, structure, and applications. Chemical Society Reviews. 2016;45(8):2327-67.
27. Hashemzadeh A, Amini MM, Tayebee R, Sadeghian A, Durndell LJ, Isaacs MA, et al. A magnetically-separable H 3 PW 12 O 40 @Fe3O4 /EN-MIL-101 catalyst for the one-pot solventless synthesis of 2H-indazolo[2,1- b] phthalazine-triones. Molecular Catalysis. 2017;440:96-106.